Solar Physics (2024) 299:126
https://doi.org/10.1007/s11207-024-02350-7

RESEARCH

The "SEP Clock": A Discussion of First Proton Arrival Times in Wide-Spread Solar Energetic Particle Events

A. Posner[1,2] · I.G. Richardson[3,4] · R.D.-T. Strauss[5]

Received: 28 March 2024 / Accepted: 17 July 2024

Abstract
This work analyzes the appearance of wide-spread deka-MeV solar energetic proton (SEP) events, in particular the arrival of the first protons within $\approx 4.5-45$ MeV measured at Earth–Sun L1, and their relationship with their relative solar source longitude. The definition of "wide-spread SEP event" for this study refers to events that are observed as a 25 MeV proton intensity increase at near 1 AU locations that are separated by at least 130° in solar longitude. Many of these events are seen at all three of the spacecraft, STEREO (Solar-Terrestrial Relations Observatory) A, STEREO B, and SOHO (Solar and Heliospheric Observatory), and may therefore extend far beyond 130° in longitude around the Sun. A large subset of these events have already been part of a study by Richardson et al. (*Solar Phys.*, **289**, 3059, 2014). The event source region identifications draw from this study; more recent events have also been added. Our focus is on answering two specific questions: (1) What is the maximum longitude over which SEP protons show energy dispersion, i.e., a clear sign of arrival of higher-energy protons before those of lower energy? (2) What implications can be drawn from the ensemble of events observed regarding either direct magnetic connectivity to shocks and/or cross-field transport from the site of the eruption in the onset phase of the event?

Keywords Solar energetic particles · Particle transport · Solar radio bursts

✉ A. Posner
arik.posner@nasa.gov

I.G. Richardson
ian.g.richardson@nasa.gov

R.D.-T. Strauss
dutoit.strauss@nwu.ac.za

1 SMD/Heliophysics Division, NASA/HQ, Washington, DC, 20546, USA

2 SRAG/Space Medicine Operations Division, NASA/JSC, Houston, TX 77058, USA

3 Dept. Astronomy, Univ. Maryland, College Park, MD, 20742, USA

4 Heliophysics Science Division, NASA GSFC, Greenbelt, MD, 20771, USA

5 Space Res. Center, Northwest Univ., Potchefstroom 2531, South Africa

Published online: 20 September 2024

1. Introduction

The onsets of solar proton events potentially contain information about physical processes acting on the protons, such as acceleration, and scattering, focusing, and drift while interacting with magnetic fields between the acceleration site and the observer. Many authors have used the signature of energy dispersion to derive the magnetic field line length of the first arriving particles, by using the $1/v$ method (being v the particle speed) for energetic electrons (Lin, Evans, and Fainberg 1973) and protons (Dresing et al. 2023), with the underlying assumption that energetic particles, following a simultaneous "release" for particles at all energies, are bound to magnetic field lines in the solar wind. This view is seemingly supported by the finding of dropouts in so-called "impulsive" solar particle events (Mazur et al. 2000) that were observed in the range of up to $\approx$200 keV. However, solar energetic particle {SEP) events have been observed that reach all solar longitudes (Dresing et al. 2023; Kollhoff et al. 2021; Richardson et al. 2014), and would do so by crossing sector boundaries (Kallenrode 1993). Therefore, if particles strictly follow magnetic field lines, the particle acceleration source would have to be nearly equally wide as the observed SEP event. In this view, wide-spread SEP events would be inconsistent with a spatially limited acceleration source such as a flaring region or jet, but more consistent with a wide source such as a travelling and expanding shock wave. The derived field line lengths often significantly exceed the assumed length of the Parker spiral (e.g. Paassilta et al., 2017, 2018). This observation is often interpreted as caused by large-scale excursions of the magnetic field in the solar wind. Another interpretation is that small-scale irregularities effectively lengthen the field line as compared to the average ideal Parker spiral (Ragot 2006), while requiring particles to strictly follow these turbulent field lines at small scales.

However, there are problems with the above view. Richardson et al. (2014) have derived arrival times of 25 MeV protons and relativistic electrons for all three-spacecraft (SOHO, STEREO A and B) events at 1 AU between the launch of STEREO and the end of 2013. The arrival times of the two particle species of vastly different speeds ($\approx$10% of c vs. $\approx$99% of c, with c the speed of light) indicate that the expansion and establishment of magnetic connectivity to the three distributed spacecraft are inconsistent. Kallenrode (1993) came to similar conclusions analyzing Helios and IMP-8 observations. In fact, there would be a need for two acceleration drivers, one that expands faster to capture the faster-occurring onsets of electrons, and one for the $\approx$25 MeV protons that expands much more slowly from the source of the solar magnetic eruption. Kollhoff et al. (2021) found that from any combination of three spacecraft chosen from Solar Orbiter, Parker Solar Probe, STEREO A, and SOHO, for the event of 29 Nov. 2020, the arrival time of electrons and 25 MeV protons can be inferred for the fourth spacecraft. Here also, if one assumes that particles strictly follow magnetic field lines, two acceleration drivers would be needed, one for relativistic electrons and the other for 25 MeV protons. An alternative view is that there is a single acceleration driver and (1) cross-field transport in the heliosphere plays a dominant role in shaping onset delays of particle events and (2) that the expansion of particle events in longitude is a function of particle speed (Strauss et al. 2023). However, in the standard spatial diffusion approach, the effect of 3D cross-field diffusion on the duration of propagation from the source to the observer is a challenge that is not yet resolved (Strauss and Fichtner 2015; Laitinen and Dalla 2019). The field-line random walk model includes an assumption that offers a way to address this problem that is not inconsistent with the observations. Here, the turbulent magnetic field lines make random excursions perpendicular to the mean magnetic field. The energetic particles then follow these turbulent magnetic fields and, in doing so, also move, in a random fashion, perpendicular to the mean magnetic field which

leads to perpendicular particle diffusion. The rate at which the particles spread perpendicular to the mean field is therefore proportional to the particle speed and leads to a perpendicular diffusion coefficient that is also proportional to the particle speed. However, transport across sector boundaries, which field lines are not expected to cross, can pose a challenge to this underlying assumption.

To test both views, we analyze the arrival time durations (i.e., the time difference between the onsets) of protons at different particle energies, not for single events, but as an ensemble of events with differing source longitudes with respect to the observer. This test could distinguish between the two views, as the analysis is limited to a single particle species, protons, whereas Kollhoff et al. (2021), Richardson et al. (2014) and Kallenrode (1993) compared electrons and protons. The goal of our study is to rule out any confusion related to multiple acceleration drivers responsible for their acceleration.

Section 2 introduces the underlying observations. In Section 3 we discuss the observations, including the dependence of proton energy dispersion on solar source longitude. Section 4 summarizes our results.

2. Observations

We have mainly analyzed proton observations of the SOHO/Comprehensive Suprathermal and Energetic Particle Analyzer (COSTEP) Electron Proton Helium Instrument (EPHIN, Müller-Mellin et al. 1995). The EPHIN instrument provides rates for predefined electron, proton, and helium channels, defined by the penetration depth (x) of particles in the solid-state detector stack that is surrounded by an active and very effective anticoincidence system. A statistical subset of particles measured are fully pulse-height analyzed, i.e., their energy (E) losses in all detectors reached are recorded. We use the combination of dE/dx vs. E pulse-height analysis and count rates to derive proton fluxes for custom channels for protons every two minutes. Kühl et al. (2020) contrast the clean proton SEP onset measurements from EPHIN with those of passively shielded instruments such as the Geostationary Operational Environmental Satellite (GOES) Energetic Particle Sensors (EPS). To provide context for the proton observations, we also consider observations of electrons made by EPHIN. Electrons are treated similarly, but due to their scattering behavior in the instrument, the derived fluxes require a response function derived from Monte Carlo simulations. As a result, the instrument provides high-quality energetic electron and proton observations in the range of 160 keV – 9 MeV and $\approx$ 4 – 53 MeV, respectively. EPHIN was mounted on the spacecraft to view along the nominal Parker spiral, westward of the Sun at 45°, with an aperture cone of 64.5° full width. However, a communications antenna issue occurred, leading to a decision to alternately roll the spacecraft by 180°, therefore, starting in July 2003, half the time EPHIN views near-perpendicular to the Parker spiral direction, towards 45° east of the Earth–Sun line (see https://soho.nascom.nasa.gov/data/ancillary/attitude/roll/nominal_roll_attitude.dat).

A more detailed description of the instrument, and the usage and limitations of the data have been discussed in detail in Sections 2 and 3 and the Appendix of Posner (2007).

We also base this study on observations that are listed in Richardson et al. (2014). These involve the identification of electron and proton events with the STEREO A and B High-Energy Telescopes (HETs, von Rosenvinge et al. 2008), and the identification of their source longitudes with a combination of extreme ultraviolet (EUV), coronagraphic and X-ray remote sensing by STEREO/Sun Earth Connection Coronal and Heliospheric Investigation

(SECCHI), Solar Dynamics Observatory/Advanced Imaging Assembly (SDO/AIA), and GOES.

Moreover, we use Wind/Solar Wind Experiment (SWE, Ogilvie et al. 1995) solar wind speed observations for inferring the magnetic footpoint longitude of SOHO and Wind (both in orbit around L1) at the solar source surface, and Wind/WAVES radio observations of type III radio bursts in the 20 kHz – 15 MHz range for the identification of the times when particles start leaving the solar corona, also taking into account equivalent observations from STEREO/SWAVES (see Appendix). Data are publicly available from the NASA CDA Web (cdaweb.gsfc.nasa.gov). In one instance, we augmented the SOHO relativistic electron observations with Wind/3D Plasma Analyzer (3DP) data for the identification of relativistic electron arrival at the Earth.

3. Solar Particle Event Selection and Analysis

A comprehensive ≈ 25 MeV solar proton event list has been published in Richardson et al. (2014) and has since been kept up to date to include more recent events (Richardson 2024). In this list, SEP proton events are identified in the cross-calibrated data sets of SOHO/COSTEP EPHIN and STEREO A and STEREO B HET. The process of identification excludes proton enhancements that are associated with the arrival of disturbances such as shocks at the spacecraft. Remote-sensing observations are used to identify the source location of the particle event. The process is explained in detail in Richardson et al. (2014).

This study identifies a subset of events from the list. We require that detecting spacecraft are separated by $> 130°$ in longitude at 1 AU, and that SOHO is one of the spacecraft detecting the particle event. Valid periods are for combinations of SOHO and STEREO A: 5 Feb. 2013 – 12 Aug. 2017, of SOHO and STEREO B: 21 Dec. 2012 – Oct. 2014 (i.e., loss of STEREO B), and for all three spacecraft: 16 Dec. 2009 – 8 Apr. 2012. This reduces the event selection to 52 events.

Energy dispersion analysis focuses on the proton spectrograms of SOHO/COSTEP EPHIN, using three energy ranges: $\approx 4 – 5$ MeV, $\approx 9 – 11$ MeV, and $\approx 40 – 53$ MeV. Figure 1 shows an example of the determination of the proton onset times for the particle event of 22 Sep. 2014. It is preceded by the onset of a type III radio burst identified in Wind/WAVES data at 06:15UT, which is marked by a red vertical line in the electron and proton spectrograms. The electron spectrogram is displayed in energy (160 keV – 8 MeV) vs. time, whereas the proton spectrogram is displayed in $1/v$ vs. time. The time range of Figure 1 starts two hours before the radio burst onset and covers 24 hours total. The time–intensity diagrams at the bottom display the intensities of the adjacent energy bins of the proton spectrogram (top two, eighth and ninth from top, bottom two). The determination of the onset time and error is performed through a combination of visual inspection and onset interval fitting of the log value of the intensities. Any intervals without particle counts are filled with the average pre-event proton intensity value that is determined during the two hours preceding the type III radio burst onset. The onset time for the fits is then determined by locating the intersection of each energy bin with the pre-event background value. The average time of two fits and visual inspection determines the onset time, and the standard deviation of the three values determines the error.

SOHO's magnetic connection longitude difference from the SEP source longitude is determined by using the Wind/SWE solar wind speed averaged over the duration spanning from the type III radio burst onset to the end of the observed proton energy dispersion period at 4.5 MeV. It is assumed that the inherent uncertainty of this method, which assumes

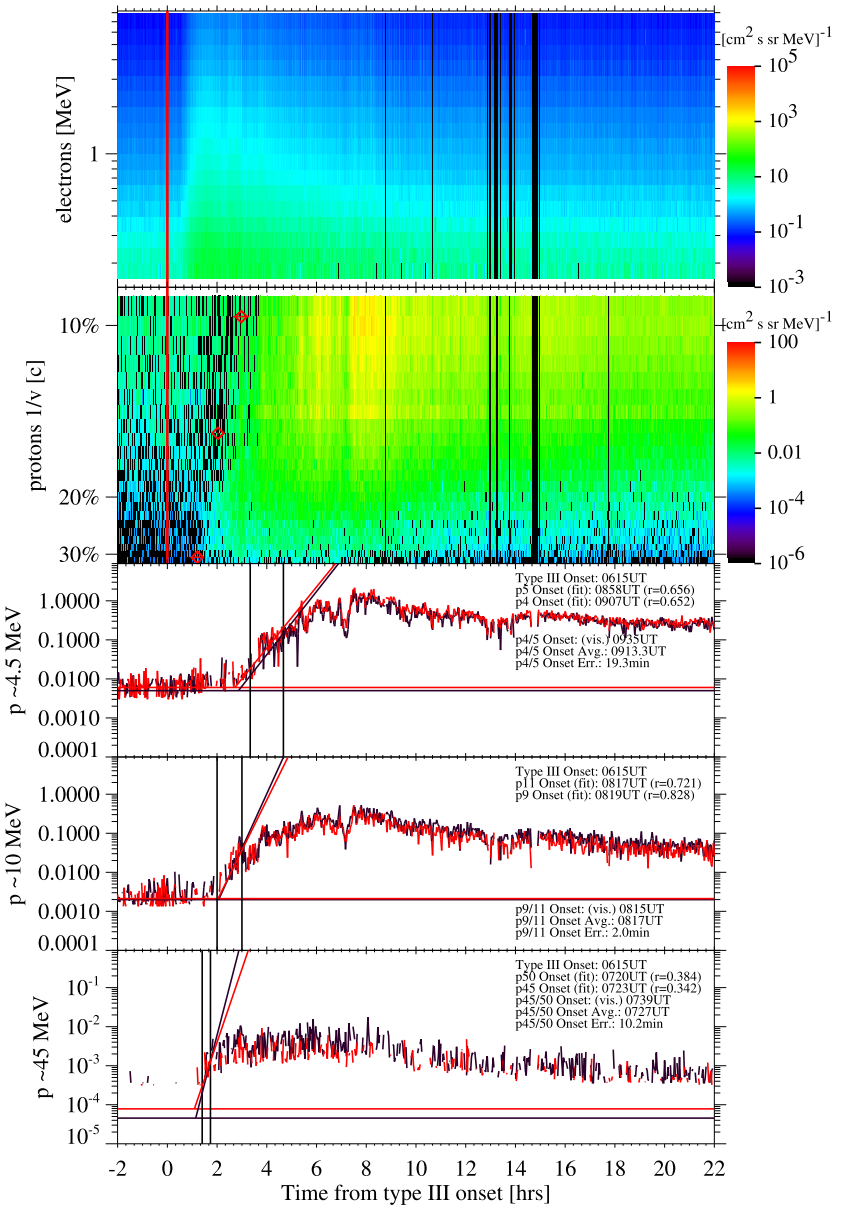

Figure 1 24-hr solar energetic electron and ion event of 22 Sept. 2014 (starting at 14 Sept. 4:15UT). Top panel: Energetic electron spectrogram (160 keV – 8 MeV). The vertical line marks the onset of the related type III radio burst. Second panel: Energetic proton spectrogram (4 – 53 MeV) in $1/v$ format. Symbols indicate inferred onset times. Third to fifth panels: Three adjacent-energy proton time-intensity profiles. The left vertical bars mark the visually inspected onset times at 4.5 MeV and the right bars mark the ends of periods in which exponential particle increases linked with the onsets occur. Visual inspection and linear fits to logs of intensities, i.e., the intersections of the fits with the pre-event backgrounds are used for determining the onset times. The horizontal lines mark the pre-event proton intensities for the lower (black) and higher (red) energy channels. Text entries provide onset times, least-squares fit correlations, and standard deviation errors for the onset time determinations.

constant speed from the Sun to 1 AU and neglects nonradial fields in the solar corona and uncertainty in the source longitude (which may be extended and not a point source) is $\approx 15°$, but this could be larger. Lario et al. (2017) discussed this problem by analyzing several methods of determining the solar footpoint of the Earth, STEREO A and B for the event of 14 Aug. 2010, including the Parker spiral method applied here, and methods that model coronal fields and/or the solar wind based on solar surface magnetograms. They found that the footpoints obtained by these methods disagreed by up to 36° in longitude, partially arising from magnetogram data age and quality. Seven of the 12 independent measurements determined by Lario et al. (2017) shown in their Table 1 are within the error we propose here, while five are outside, which lends credibility to our suggested uncertainty in the footpoint longitude.

Table 1 lists data products of all 52 events in chronological order. Events in which the EPHIN instrument is pointed perpendicular to the nominal magnetic field are indicated by an asterisk. The table contains the source locations, durations of energy dispersion, including the event discussed above (No. 48 in the table), and times of identified type III and electron event onsets. Missing onset times are indicated by N/A. The presence or absence of type II radio bursts is also provided.

Theoretical minimum delays from field-aligned propagation from the Sun to 1 AU related to these energy intervals are listed in Table 2, for three common solar wind speed ranges, assuming a Parker spiral and that particles of each energy are injected onto the field line simultaneously.

Of the 52 wide-spread events listed in Table 1, 30 originate from inside the solar radiation hemisphere (SRH), which is defined in Posner et al. (2021) as the hemisphere of the Sun that is centered around W60, spanning from E30 to W150. Twenty-two events originate from outside the SRH. One of the events, No. 36, carries a caveat, as it is listed with a source at E58, but there is near-simultaneous sympathetic solar activity in the well-connected western hemisphere of the Sun that may have caused the small SEP event observed at SOHO. Given the ambiguity, we omit this event from further consideration, reducing the total number of events analyzed to 51 and those from outside the SRH to 21. Figure 2 shows histograms of proton intensities at SOHO distinguished by their origin within (top) or outside (bottom) the solar radiation hemisphere. There is a clear ordering of high local intensity from SEP events that originate from inside the SRH. These events have small magnetic connection distances from the source of the solar activity, in particular when compared to SEPs originating outside the SRH.

Eighty per cent of the SRH SEP events are accompanied by heliospheric type II radio burst activity observed by the STEREO and/or Wind spacecraft (see https://cdaw.gsfc.nasa.gov/CME_list/radio/waves_type2.html). The existence of a deka-/hectometric type II emission is indicative of a coronal mass ejection (CME)-driven shock accelerating electrons. The CMEs in our sample with such type IIs are on average faster (1,300 km/s) and wider (335°) than non-type II producing CMEs (894 km/s, 305°). Non-SRH SEP events are accompanied by heliospheric type II radio bursts only at a rate of 71%. While the statistical sample is small, it is surprising that we observe any SEPs without such signatures from the non-SRH in view of the literature (e.g. Rouillard et al. 2012) requiring broad CME shocks to reach observers that are not well connected to the source location.

Eighty per cent of SRH SEP events show clear signatures of proton energy dispersion in the $\approx 4.5-45$ MeV range at SOHO. Note that this and the type II-distribution originating in the SRH are overlapping but non-identical. A much lower percentage of non-SRH SEP events (52%) has clearly recognizable proton energy dispersion. This is not surprising given the much lower relative maximum intensities, which are reflected in correspondingly lower intensity ramps near the onset. If an elevated pre-event particle intensity is present locally,

Table 1 List of all SEP events with >25 MeV protons for which SOHO and at least one STEREO spacecraft were separated by 130°. Numbered events, asterisks marking events in which EPHIN viewed away from the nominal Parker spiral, are identified by the time of the type III radio burst onset. The presence/absence of a type II burst is taken from Richardson et al. (2014). Onset times of relativistic electrons and 4 – 53 MeV protons at SOHO are listed, including durations of onsets (i.e., onset duration here is the time between onsets at the different energies) where available, but for event No. 34 taken from Wind/3DP due to a data gap. For a multitude of reasons, there is a large subset of SEP proton events for which the onset time cannot be accurately determined ("N/A"). The reasons are identified in the table as: (a) faint events, (b) events that do not reach the highest proton energy/energies, (c) intermittent local solar wind structures interfering with onset, (d) pre-event background with small signal-to-noise ratio, (e) data gaps. Magnetic field rotations that may have influenced the onset time determination are marked with # in the onset time and duration fields.

Ev. No.	Date	Time Type III Onset [UT]	p+ Intens. Max. [cm s sr MeV]$^{-1}$	Source Long. [^{o}]	Conn. Dist. [^{o}]	e- Onset [UT]	Type II?	p+ 45 MeV Onset [UT]	p+ 10 MeV Onset [UT]	p+ 4.5 MeV Onset [UT]	Dur. 45 MeV – 4.5 MeV [min]	Dur. 45 MeV – 10 MeV [min]	Dur. 10 MeV – 4.5 MeV [min]
1*	22 Dec. 2009	04:55	0.0005	W40	31	05:38	N	N/A$^{(a)}$	N/A$^{(a)}$	N/A$^{(a)}$	N/A$^{(a)}$	N/A$^{(a)}$	N/A$^{(a)}$
2	14 Aug. 2010	10:03	0.2	W54	3	10:18	N	10:39 ± 7	11:09 ± 21	12:01 ± 13	80 ± 20	30 ± 28	52 ± 33
3	18 Aug. 2010	05:39	0.03	W100	-33	06:02	Y	N/A$^{(b)}$	07:36 ± 3	08:28 ± 12	N/A$^{(b)}$	N/A$^{(b)}$	52 ± 14
4	31 Aug. 2010	20:52	0.005	W145	-71	21:16	Y	N/A$^{(b)}$	23:53 ± 5	01:30 ± 5	N/A$^{(b)}$	N/A$^{(b)}$	97 ± 10
5	8 Sept. 2010	23:29	0.003	W92	-22	23:42	Y	N/A$^{(b)}$	01:12 ± 15	02:08 ± 1	N/A$^{(b)}$	N/A$^{(b)}$	56 ± 16
6	21 Mar. 2011	02:20	0.11	W138	-69	03:00	Y	03:34 ± 9	04:17 ± 20	05:02 ± 16	88 ± 25	43 ± 29	45 ± 36
7*	4 Jun. 2011	22:04	0.04	W165	-117	22:24	Y	N/A$^{(c)}$	N/A$^{(c)}$	N/A$^{(c)}$	N/A$^{(c)}$	N/A$^{(c)}$	N/A$^{(c)}$
8	4 Aug. 2011	03:51	1.1	W36	35	04:24	Y	05:11$^{\#}$ ± 6	05:47 ± 7	06:40 ± 14	89$^{\#}$ ± 19	36$^{\#}$ ± 13	53 ± 21
9	6 Sept. 2011	22:22	0.1	W18	43	22:58	Y	23:58 ± 12	01:14 ± 12	01:59 ± 18	121 ± 30	76 ± 24	45 ± 30
10*	3 Nov. 2011	22:24	0.04	E152	-135	23:00	Y	23:28$^{\#}$ ± 5	00:24 ± 2	01:32 ± 21	124$^{\#}$ ± 25	56$^{\#}$ ± 7	68 ± 23
11*	26 Nov. 2011	07:11	0.3	W48	13	07:24	Y	N/A$^{(c)}$	N/A$^{(c)}$	N/A$^{(c)}$	N/A$^{(c)}$	N/A$^{(c)}$	N/A$^{(c)}$
12	23 Jan. 2012	03:40	20.	W21	33	04:00	Y	04:36 ± 4	05:39 ± 3	06:17$^{\#}$ ± 6	102$^{\#}$ ± 10	63 ± 7	39$^{\#}$ ± 10
13*	17 May 2012	01:33	0.6	W76	-8	01:56	Y	03:10 ± 8	04:52 ± 8	06:39 ± 21	208 ± 29	102 ± 16	106 ± 29
14*	26 May 2012	20:48	0.03	W116	-48	21:06	Y	21:54 ± 5	22:44 ± 6	23:46 ± 4	112 ± 9	50 ± 11	62 ± 9
15	23 Jul. 2012	02:12	0.2	W140	-84	05:20	Y	06:05 ± 3	N/A$^{(c,d)}$	N/A$^{(c,d)}$	N/A$^{(c,d)}$	N/A$^{(c,d)}$	N/A$^{(c,d)}$
16	31 Aug. 2012	19:50	0.04	E42	121	20:40	Y	N/A$^{(b)}$	22:48$^{\#}$ ± 13	00:32$^{\#}$ ± 45	N/A$^{(b)}$	N/A$^{(b)}$	105$^{\#}$ ± 58
17	20 Sept. 2012	14:57	0.003	E158	-153	22:00	Y	N/A$^{(a)}$	N/A$^{(a)}$	N/A$^{(a)}$	N/A$^{(a)}$	N/A$^{(a)}$	N/A$^{(a)}$
18	26 Feb. 2013	10:08	0.01	W131	-54	11:20	Y	N/A$^{(b)}$	12:16 ± 15	N/A$^{(d)}$	N/A$^{(b,d)}$	N/A$^{(b)}$	N/A$^{(d)}$

Table 1 (*Continued*)

Ev. No.	Date	Time Type III Onset [UT]	p+ Intens. Max. [cm s sr MeV]$^{-1}$	Source Long. [^{o}]	Conn. Dist. [^{o}]	e- Onset [UT]	Type II?	p+ 45 MeV Onset [UT]	p+ 10 MeV Onset [UT]	p+ 4.5 MeV Onset [UT]	Dur. 45 MeV – 4.5 MeV [min]	Dur. 45 MeV – 10 MeV [min]	Dur. 10 MeV – 4.5 MeV [min]
19	5 Mar. 2013	03:43	0.006	E141	-151	07:30	Y	N/A$^{(a,d)}$	N/A$^{(a,d)}$	N/A$^{(a,d)}$	N/A$^{(a,d)}$	N/A$^{(a,d)}$	N/A$^{(a,d)}$
20*	11 Apr. 2013	06:56	2.	E12	72	07:42	Y	08:12 ± 8	08:56$^{\#}$ ± 15	10:52 ± 5	150 ± 13	44$^{\#}$ ± 23	116$^{\#}$ ± 20
21*	21 Apr. 2013	07:30	0.02	W124	-36	08:10	N	N/A$^{(b)}$	N/A$^{(d)}$	N/A$^{(d)}$	N/A$^{(b,d)}$	N/A$^{(b,d)}$	N/A$^{(d)}$
22*	24 Apr. 2013	21:38	0.01	W175	-116	22:12	N	22:46 ± 26	00:05 ± 117	N/A$^{(d)}$	N/A$^{(d)}$	71 ± 143	N/A$^{(d)}$
23*	13 May 2013	15:56	0.01	E95	162	17:36	Y	18:17 ± 132	22:09$^{\#}$ ± 35	02:38$^{\#}$ ± 17	560$^{\#}$ ± 149	292$^{\#}$ ± 167	269$^{\#}$ ± 52
24*	22 May 2013	13:10	20.	W70	-15	13:42	Y	13:55$^{\#}$ ± 24	14:40 ± 7	15:10 ± 3	68$^{\#}$ ± 26	45$^{\#}$ ± 31	30 ± 10
25*	21 Jun. 2013	02:55	0.06	E73	124	06:00	Y	N/A$^{(b)}$	12:23 ± 28	16:18 ± 84	N/A$^{(b)}$	N/A$^{(b)}$	236 ± 112
26	22 Jul. 2013	06:32	0.001	W172	-106	08:06	N	08:56 ± 23	10:35 ± 3	12:21 ± 115	206 ± 138	99 ± 26	107 ± 118
27	19 Aug. 2013	23:13	0.01	W174	-116	01:00 (+1d)	Y	N/A$^{(b)}$	N/A$^{(b,d)}$	N/A$^{(d)}$	N/A$^{(b,d)}$	N/A$^{(b,d)}$	N/A$^{(b,d)}$
28	29 Sept. 2013	21:55	0.5	W25	67	22:22	Y	22:49 ± 27	23:36 ± 3	00:25 ± 21	96 ± 48	47 ± 30	49 ± 24
29*	11 Oct. 2013	07:14	0.002	E96	159	14:00	Y	N/A$^{(a,d)}$	N/A$^{(a,d)}$	N/A$^{(a,d)}$	N/A$^{(a,d)}$	N/A$^{(a,d)}$	N/A$^{(a,d)}$
30*	2 Nov. 2013	04:32	0.02	W127	-53	06:00	N	07:12 ± 20	N/A$^{(d)}$	N/A$^{(d)}$	N/A$^{(d)}$	N/A$^{(d)}$	N/A$^{(d)}$
31*	19 Nov. 2013	10:24	0.04	W69	-4	10:40	Y	11:26 ± 2	12:20 ± 4	12:52 ± 10	87 ± 12	54 ± 5	32 ± 14
32*	14 Dec. 2013	06:25	0.002	E144	-155	09:00	N	N/A$^{(d)}$	N/A$^{(d)}$	N/A$^{(d)}$	N/A$^{(d)}$	N/A$^{(d)}$	N/A$^{(d)}$
33*	26 Dec. 2013	02:54	0.03	E161	-110	04:30	N	N/A$^{(b)}$	05:56$^{\#}$ ± 2	06:48$^{\#}$ ± 13	N/A$^{(b)}$	N/A$^{(b)}$	53$^{\#}$ ± 15
34*	6 Jan. 2014	07:48	0.6	W110	*-46*	*08:25*$^{(e)}$	Y	N/A$^{(e)}$	09:34 ± 11	10:44 ± 6	N/A$^{(e)}$	N/A$^{(e)}$	70 ± 17
35	7 Jan. 2014	18:07	2.2	W11	56	19:00	Y	19:30 ± 4	20:16 ± 26	21:38 ± 36	128 ± 41	46 ± 31	82 ± 103
36	*30 Jan. 2014*	*16:03*	*0.002*	*E58*$^{(e)}$	*125*	*16:50*	*N*	*N/A*$^{(b)}$	*18:03 ± 17*	*18:39 ± 6*	*N/A*$^{(b)}$	*N/A*$^{(b)}$	*37 ± 22*
37	14 Feb. 2014	08:22	0.003	W147	-76	09:40	N	N/A$^{(d)}$	N/A$^{(d)}$	N/A$^{(d)}$	N/A$^{(d)}$	N/A$^{(d)}$	N/A$^{(d)}$
38	18 Feb. 2014	01:20	0.004	E45	115	03:50	Y	N/A$^{(b)}$	N/A$^{(d)}$	N/A$^{(d)}$	N/A$^{(b,d)}$	N/A$^{(b,d)}$	N/A$^{(d)}$
39	21 Feb. 2014	15:44	0.001	E120	172	20:00	N	N/A$^{(d)}$	N/A$^{(d)}$	N/A$^{(d)}$	N/A$^{(d)}$	N/A$^{(d)}$	N/A$^{(d)}$
40	25 Feb. 2014	00:47	0.3	E82	139	02:02	Y	03:40 ± 25	08:06 ± 36	13:17 ± 10	577 ± 35	266 ± 62	311 ± 46

Table 1 (*Continued*)

Ev. No.	Date	Time Type III Onset [UT]	p+ Intens. Max. [cm s sr MeV]$^{-1}$	Source Long. [^{o}]	Conn. Dist. [^{o}]	e- Onset [UT]	Type II?	p+ 45 MeV Onset [UT]	p+ 10 MeV Onset [UT]	p+ 4.5 MeV Onset [UT]	Dur. 45 MeV – 4.5 MeV [min]	Dur. 45 MeV – 10 MeV [min]	Dur. 10 MeV – 4.5 MeV [min]
41*	28 Mar. 2014	23:22	0.001	W23	34	00:02 (+1d)	Y	N/A$^{(b)}$	02:26 ± 10	02:43$^{\#}$ ± 8	N/A$^{(b)}$	N/A$^{(b)}$	18$^{\#}$ ± 18
42*	29 Mar. 2014	17:46	0.03	W32	26	18:06	Y	18:44 ± 2	19:26 ± 4	19:50$^{\#}$ ± 34	66$^{\#}$ ± 36	41 ± 6	24$^{\#}$ ± 38
43*	2 Apr. 2014	13:28	0.001	E53	116	19:00	Y	N/A$^{(d)}$	N/A$^{(d)}$	N/A$^{(d)}$	N/A$^{(d)}$	N/A$^{(d)}$	N/A$^{(d)}$
44*	9 May 2014	02:22	0.003	W110	-44	03:50	Y	N/A$^{(b)}$	04:46 ± 14	05:47 ± 7	N/A$^{(b)}$	N/A$^{(b)}$	61 ± 21
45	8 Jul. 2014	16:12	0.0005	E56	132	16:58	N	17:12 ± 1	18:37 ± 13	19:27 ± 10	135 ± 11	86 ± 14	50 ± 23
46	1 Sept. 2014	11:03	0.02	E108	169	14:40	Y	21:43 ± 63	02:04 ± 55	06:33 ± 47	530 ± 111	261 ± 119	269 ± 103
47	10 Sept. 2014	17:30	0.4	E02	68	18:45	Y	N/A$^{(d)}$	N/A$^{(d)}$	N/A$^{(d)}$	N/A$^{(d)}$	N/A$^{(d)}$	N/A$^{(d)}$
48	22 Sept. 2014	06:15	0.03	W149	-91	06:48	Y	07:27 ± 10	08:17 ± 2	09:13 ± 19	106 ± 40	50 ± 12	56 ± 21
49*	24 Sept. 2014	20:50	0.003	W179	-123	23:00	Y	N/A$^{(d)}$	N/A$^{(d)}$	N/A$^{(d)}$	N/A$^{(d)}$	N/A$^{(d)}$	N/A$^{(d)}$
50*	29 Oct. 2015	02:19	0.2	W95	-13	02:36	N	03:04 ± 16	03:56 ± 17	04:32 ± 15	88 ± 31	51 ± 33	36 ± 32
51*	9 Nov. 2015	13:06	0.04	E39	85	14:50	Y	15:02 ± 27	18:20 ± 6	19:48 ± 6	286 ± 33	198 ± 33	89 ± 12
52	23 Jul. 2017	05:01	0.01	W148	-105	07:40	Y	N/A$^{(d)}$	N/A$^{(d)}$	N/A$^{(d)}$	N/A$^{(d)}$	N/A$^{(d)}$	N/A$^{(d)}$

Table 2 The table lists the expected delay durations between arrivals of protons of the energy ranges listed on the left, for various typical solar wind speeds. The distance to the Sun along the Parker spiral is also provided. The minimum delays are included in Figures 4 and 6 as horizontal lines.

Proton Energy Interval	Delay Duration Vsw: 300 km/s	Delay Duration Vsw: 400 km/s	Delay Duration Vsw: 500 km/s
45 – 4.5 MeV	72.9 min	67.5 min	65.3 min
45 – 10 MeV	37.8 min	35.0 min	33.8 min
10 – 4.5 MeV	35.1 min	32.5 min	31.5 min
Ideal Parker Spiral Length	*1.26 AU*	*1.16 AU*	*1.12 AU*

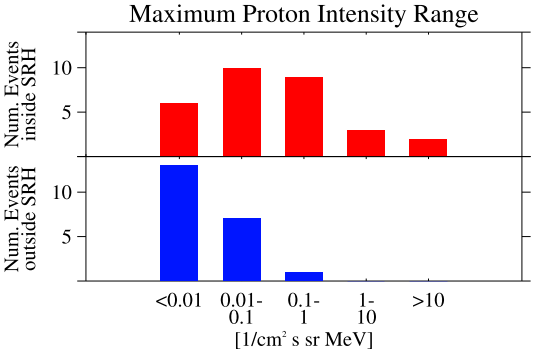

Figure 2 Number of events of Table 1 with maximum 25 MeV proton intensity at or below the thresholds in the unit of $[\text{cm}^2\ \text{s sr MeV}]^{-1}$. The top panel is for events that originate in solar activity occurring within the solar radiation hemisphere of longitude range E30 to W150, which is centered around W60 of the Sun's central meridian as viewed from the Earth. The bottom panel shows the intensity distribution of events originating from the opposite solar hemisphere. Solar source longitudes and proton intensities were identified by Richardson et al. (2014).

the onset energy dispersion of weaker-appearing events would have a lower signal-to-noise level and would be more difficult to recognize. This affects the non-SRH events disproportionately. There are clear examples, events No. 46 and 23, that reveal onset dispersion despite the inferred magnetic connection distance exceeding 160° in longitude. Recognition of energy dispersion requires a combination of clean observations and quiet pre-event conditions. Under favorable circumstance, it appears likely that SEP events from anywhere on the Sun can create energy dispersion patterns of protons anywhere at 1 AU.

The durations between the arrivals of 4.5 MeV and 45 MeV protons range from about one hour to almost 10 hours. In the literature, onset dispersion signatures are being used to infer particle release time, and the length of the magnetic field line connecting the observer with the Sun (e.g. Klein and Posner 2005; Dresing et al. 2023). It is important to recognize that these two inferences require proton cross-field diffusion to be extremely low. Our statistical analysis of a large ensemble of wide-spread SEP events can test whether this assumption is generally valid. There are two (extreme) possibilities:

a) No cross-field transport of protons. In this scenario, protons can only reach the observer if a direct magnetic field line connection to the accelerating source is established. As the extended source, notably a CME-driven shock, expands into the heliosphere, it can intercept the magnetic field line that connects Earth/SOHO with the Sun. This may oc-

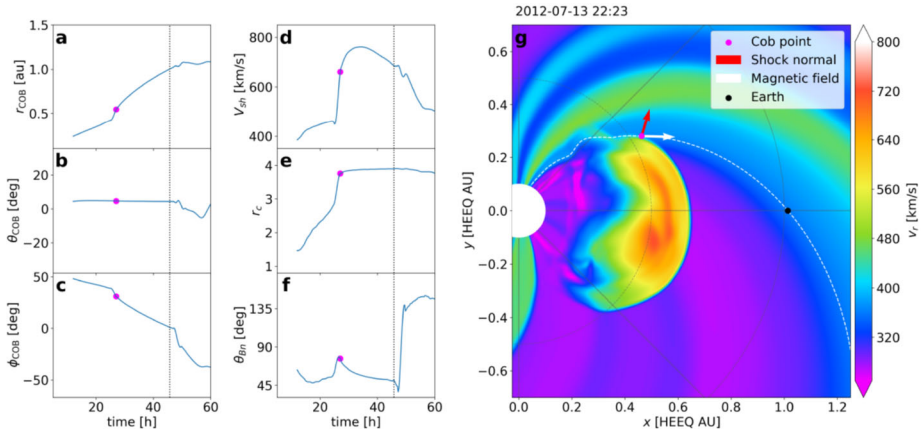

Figure 3 This figure, adapted with permission, is fully described in Wijsen et al. (2022). It shows a simulation of a CME that erupted on 12 July 2012 at around 15:00 UT along with an X1.6 flare from E6. Panel g shows the "connection with the observer" (COB) point where the field line connected to the Earth first encounters the flank of the expanding shock and illustrates the shortening of the magnetic field line length to approximately 0.6 AU between acceleration source at the COB point and observer. Panels a–c describe the location of the COB point after CME launch (radial distance, latitude, and longitude) and panels d–f describe the shock parameters at the COB point.

cur at a significant distance from the Sun, therefore shortening the magnetic field line length between the acceleration source and the 1 AU observer. From a statistical analysis one would expect shorter durations of proton energy dispersion with increasing magnetic connection distance from the SEP source. This is equivalent to a racetrack in which the arrival time is clocked between a faster and a slower car. If the racetrack is shortened, the time delay between the two arrivals is shortened proportionately. If one assumes a wide CME spanning up to 180° in longitude, the intercept of a shock with the Parker spiral would rise to a significant distance from the Sun rather quickly.

b) Particles reach regions far away from any magnetic connection to an acceleration region at the Sun via cross-field transport. This may encompass pitch angle scattering or transport across the average field by processes such as field-line random walk while within the same magnetic sector. Limiting ourselves to particle scattering, one would expect the diffusive transport away from the best-connected field line to proceed quickly. With increasing connection distance, however, the particle intensity gradient would decrease, and the process slows down, as protons become increasingly likely to be scattered back towards their longitude of origin. The diffusion process would increase the effective path length of particles, but not necessarily along existing field lines. Assuming comparable cross-field diffusion coefficients across the energy range of EPHIN for protons, the effective path length increase would be equivalent to the lengthening of the "racetrack", increasing the duration between fast- and slow-moving particles arriving at SOHO, and resulting in longer durations of proton energy dispersion.

The recent example of 12 July 2012, discussed under assumption (a), is presented in Figure 3 from Wijsen et al. (2022), using a EUHFORIA (European Heliospheric Forecasting Information Asset) simulation (Pomoell and Poedts 2018). The SEP event is not included in Table 1 as it was detected by SOHO and STEREO B when the spacecraft were less than 130° apart. The authors discuss the onset of the SEP event in the context of an established direct magnetic connection between the Earth and the "connection to the observer" (COB) point

at the flank of the shock and find that "[i]n the simulation, this observer (hereafter Earth) connects with the shock front about ≈ 30 h after the CME insertion (i.e., on 13 July, around 22:00 UT). However, the observed onset of the SEP event suggests that the Earth had likely a direct magnetic field connection to the shock wave shortly after the CME eruption (i.e., on 12 July around 17:00 UT)." The following discussion in the article considers an even wider shock, and the possibility that the magnetic field was more radial, but not the possibility that the acceleration might have occurred near the SEP origin and that the particles reached the observer predominantly through cross-field diffusion.

A related question is whether or how SEP onsets with energy dispersion can be detected from events originating in excess of ≈ 90° from the observer. A magnetic connection to a CME shock outside 1 AU (e.g. Reames, Barbier, and Ng 1996) is not a possibility, as the onset times consistently stay within one day of the solar event, and CMEs that reach 1 AU within this time have not been observed. Reports of CMEs extending beyond 180° exist. But even in this case, the average field line length connecting the observer to the overly wide CME shock would not increase, no matter what the magnetic connection distance from the SEP source is. Thus, the onset dispersion durations of well-connected events would set the upper limit for all events assuming possibility (a).

Figure 4 tests the assumptions with our statistically relevant sample of wide-spread particle events observed from nearly all magnetic connection distances. We have separated the full energy range of EPHIN into three segments (full: 4.5 – 45 MeV, high-energy: 10 – 45 MeV, low: 4.5 – 10 MeV) so that we maximize the amount of available data, since some events do not reach the highest energies considered, while for others, a pre-event background limits estimation of the energy dispersion to the higher energies.

We divide Figure 4 in three areas (yellow, green, and blue marked on the right side in each viewgraph), separated by horizontal lines that mark energy dispersion durations for full Parker field line lengths at 1 AU for a range of common solar wind speeds. We would expect the area below the lines (yellow) to be filled with energy dispersion durations from events in which raised COB points reduce the magnetic field line length, i.e., from a CME-driven shock in the heliosphere to Earth. Locations on/near the lines (green) would be populated with events in which sources equivalent to EUV waves, i.e., extended sources that do not lift above the corona, cause particle acceleration and release. These would neither reduce nor extend the magnetic field line length between particle source and observer at 1 AU. The area above the lines (blue) should only be populated by events that are dominated by the process of particle transport, a process that effectively extends the travel path independent of magnetic field line connection length.

Linear fits to the three energy ranges in Figure 4 have a positive slope, meaning that the average duration of the energy dispersion increases with increasing magnetic connection distance. Linear correlation coefficients are significant, with $r = 0.731$ for the full proton energy range (top), $r = 0.682$ for the upper energy range (middle), and $r = 0.710$ for the lower energy range (bottom). As discussed above, the sample of events with recognizable energy dispersion at large magnetic connection distances is rather limited. However, the observed events are clear cases.

Figure 5 shows representative examples of proton energy dispersion in a "solar energetic particle clock" organization, which displays electron and ion spectrograms over each of the 12 clock sectors of their source longitude with respect to the Earth at the 6 o'clock position. Events in the solar radiation hemisphere cover sectors 3 – 6 and split sectors 2 and 7 with events outside the solar radiation hemisphere. Long-duration energy dispersion events are present in sectors 7, 9, and 10, which refer to the events No. 51, 40, and 46 in Table 1.

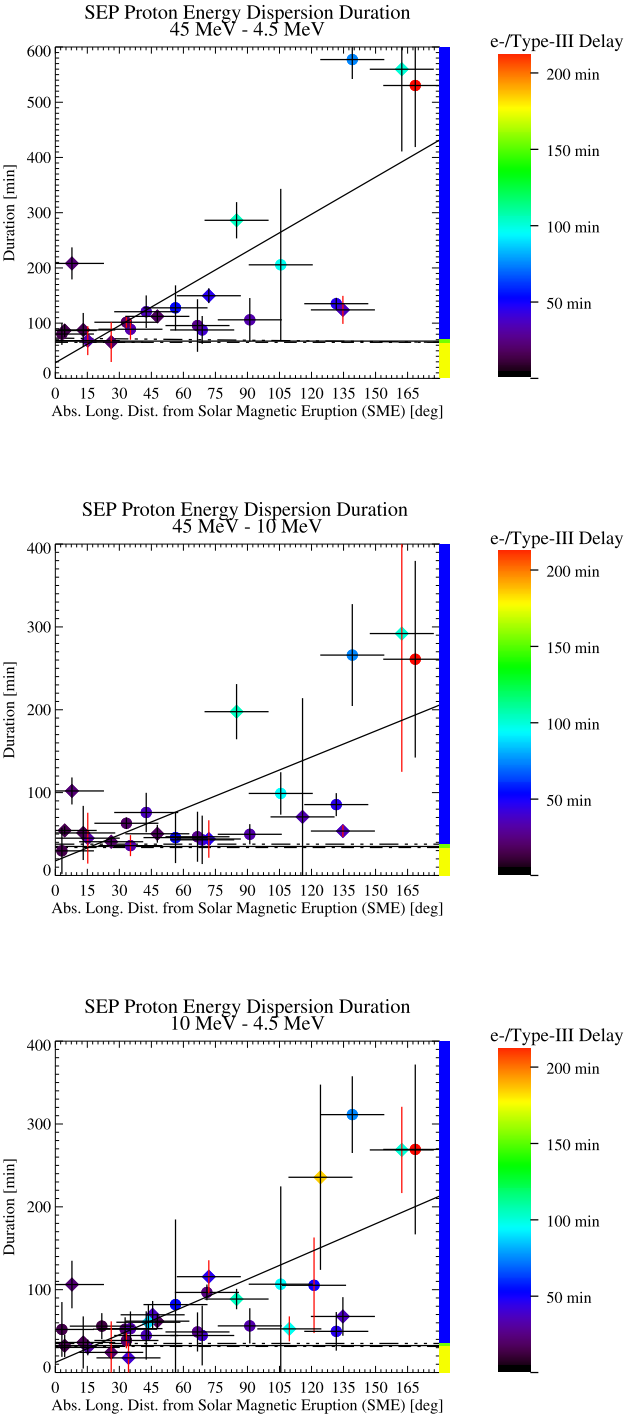

Figure 4 The graph on top displays 45 – 4.5 MeV energy dispersion durations over absolute magnetic connection distances for all events of Table 1 in which the duration can be determined. We assume a ± 15° uncertainty in the magnetic connection distance due to non-radial fields in the corona and from using the simple solar wind speed method that assumes constant speed from the Sun to 1 AU. Uncertainties in onset dispersion durations are described in the text. Circles (diamonds) depict events in which the instrument opening was aligned with (perpendicular to) the nominal Parker spiral. Duration error bars in red indicate that observed magnetic field rotations into/out of the instrument field of view may have influenced the duration. Symbols are color coded with the delay between the type III radio burst onset and the onset of relativistic electrons. The middle and bottom graphs show energy dispersion durations of 45 – 10 MeV and 10 – 4.5 MeV, respectively. Horizontal lines indicate theoretical minimum delays if particles follow the Parker spiral length from the Sun to 1 AU for solar wind speeds listed in Table 2.

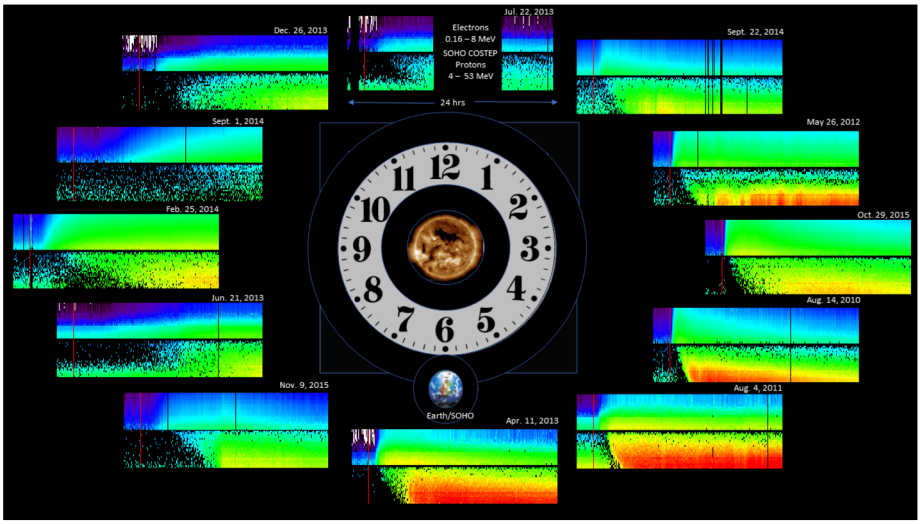

Figure 5 Solar energetic particle "clock" representation of 24-hr spectrograms of 160 keV – 8 MeV electrons (top) and 4 – 53 MeV protons (bottom) for each of the 12 clock sectors. All events were observed from SOHO in the near-Earth solar wind. The SEP events are shown over their inferred source location sector. Red vertical lines, two hours into each of the 24-hr periods shown, indicate the onset of Wind/WAVES type III radio bursts associated with the SEP events. The electron and proton intensity scales are shown in Figure 1. The associated events in Table 1 are: hr1: No. 48, hr 2: No. 14, hr 3: No. 50, hr 4: No. 2, hr 5: No. 8, hr 6: No. 20, hr 7: No. 51, hr 8: No. 25, hr 9: No. 40, hr 10: No. 46, hr 11: No. 33, hr 12: No. 26.

Richardson et al. (2014) have shown that onset time delays for electrons and for protons each at a different single energy show a positive correlation with magnetic connection distance. This tendency was also previously discussed by Kallenrode (1993). Figures 15 and 16 of Richardson et al. (2014) show that the delay can be matched by assuming a fixed duration for streaming along the field to 1 AU for each species if combined with the expansion of an inciter at the solar surface. To match, the inciter must have a higher speed for relativistic electrons than for the 25 MeV protons they analyzed. This set of observations already hints towards an alternative interpretation for the observed onset delays: particle speed dependent cross-field diffusion. Yet, as recently shown in the simulations of Strauss et al. (2023), the option of having different acceleration regions for protons and electrons driven by an expanding CME shock cannot be ruled out. Based on the observations above, we can add that the onset delays for a single species at different energies bolsters the case for the role of speed-dependent particle cross-field diffusion. In addition, an explanation of our observations by scatter-free travel from the accelerating source would require a slow exciter speed for low-energy protons and a high exciter speed for higher-energy protons, and it would require the exciter to remain at solar surface height. This seems unlikely.

We also note that longer-duration proton energy dispersion coincides with longer average delays between type III and electron onsets for the same events. This is discernible from the color coding of the events shown in Figure 4. Figure 6 contains the same information as Figure 4 but switches the way magnetic connection distance and electron onset delay are displayed. The correlation of proton energy dispersion with electron delay is visible here with $r = 0.772$ for the full proton energy range (top), $r = 0.780$ for the upper energy range (middle), and $r = 0.715$ for the lower energy range (bottom). It is, moreover, important to highlight that all long-duration proton energy dispersion events also have long delays

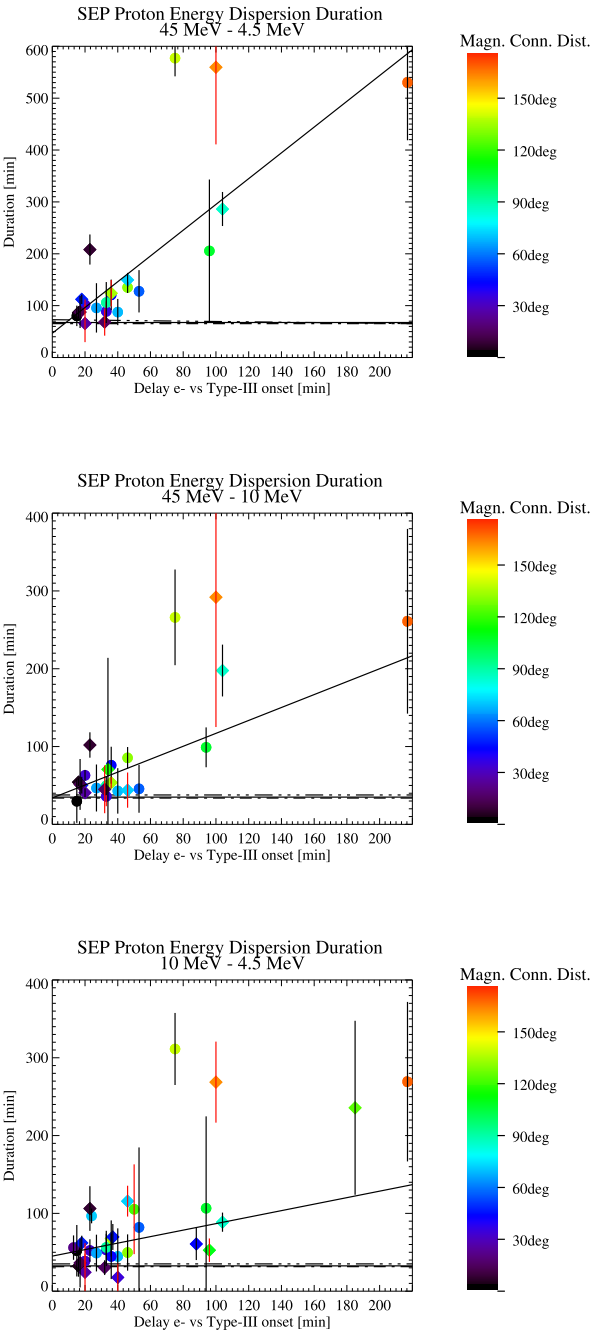

Figure 6 The same data as shown in Figure 4. Here the color coding is related to magnetic connection distance, whereas time delay of relativistic electron onset vs. type III radio burst onset is now on the horizontal axis. Horizontal lines again indicate theoretical minimum delays if particles follow the Parker spiral length from the Sun to 1 AU for solar wind speeds listed in Table 2.

of electron onsets over type III radio bursts. These two independent observations can be separated in time by >12 hours (e.g., event No. 40). This poses a challenge to view (a) in that a direct magnetic connection to a far away accelerator inside 1 AU needs to be maintained for a long time.

We further note that there are a few events for which a comparatively small delay between type III onset and electron onset suggests a shorter magnetic connection distance than listed. A possibility is that the source longitude for the protons detected at the Earth is ambiguous and different from that listed. One such event is listed as No. 10. This has been widely discussed because of the unusually rapid particle arrival at both STEREOs and at the Earth following an eruption behind the east limb associated with a CME, which was directly observed by STEREO B (Richardson et al. 2014; Gomez-Herrero et al. 2015; Zhao and Zhang 2018). While these authors have concluded that this single eruption gave rise to the widespread SEP event, we note that Park et al. (2013) and Prise et al. (2014) have proposed that a separate source gave rise to the SEP event at the Earth. However, Gomez-Herrero et al. (2015) argue on several grounds that this view is not correct. Since the poorly connected source region could be correct for this event, this suggests that other factors may influence particle propagation beyond the two scenarios considered here.

4. Discussion and Conclusions

We have used a list of multi-spacecraft solar energetic particle events (25 MeV protons) based on observations at both STEREO and near-Earth spacecraft to identify all listed widespread events that exceed 130° in solar longitude and that have been detected at SOHO near the Earth. We have analyzed the duration of proton energy dispersion at the onset of these events (i.e., the time difference between the onset at different energies).

Commonly, proton energy dispersion in individual SEP events is used in the community to infer (1) the particle release time at the Sun and (2) the length of the magnetic field line between the observer and the Sun under the assumption that protons strictly follow the magnetic field. Our analysis challenges this technique by looking at a statistical sample of events and contrasting the assumption of negligible cross-field diffusion with one in which cross-field diffusion dominates the appearance of SEP events. The dependency of the onset time duration of protons on longitude is critical for this distinction. The zero-cross-field diffusion case (case a) would require a broad acceleration region that "touches" the field line the observer is on, as discussed by Wijsen et al. (2022). This would have to occur at an increasing height above the corona as the magnetic connection distance of the observer from the source of the eruption increases. The increasing height would, in turn, shorten the magnetic field line length between the connection to the observer (COB) point and the observer and would reduce the duration of the proton energy dispersion. In contrast, our analysis supports the idea that a direct magnetic connection to the accelerating source is not needed. Rather, the onset duration is determined by the average diffusion time of protons at a given energy to reach the observer, as supported by our finding of a positive correlation between magnetic connection distance and proton onset dispersion. In summary, we conclude that the energy dispersion analysis to infer solar release times and magnetic connection field line lengths cannot be applied without caveats and is likely invalid unless used near the Sun and near the ideal magnetic connection with the accelerating source.

We have also found that SEP events can reveal proton onset dispersion even if they originate from a source region that is essentially on the opposite side of the Sun from the magnetic connection of the observer. It is extremely difficult to explain SEP events of such a width without significant particle cross-field diffusion, and even more difficult to explain why these events can have energy onset dispersion. The observed energy dispersion durations between $\approx$45 MeV protons at $\approx$30% light speed and $\approx$4.5 MeV protons at $\approx$10%

light speed extend over more than 9 hours. The magnetic field line length would need to be above 13 AU to produce this dispersion.

Strauss et al. (2023) address the large inter-event variation of electron and proton onset delays with extended acceleration sources. Similarly, we observe significant inter-event variation in proton delays between different energies. While extending the source size from 5° to 35° in longitude helps with matching some onset delays at large separation angles better, Strauss et al. cannot match occurrences of instances of extremely short onset delays in some well-connected events (their Figures 6 and 7, center panels). These hint towards significant event-to-event variations in propagation conditions, such as low-turbulence states within magnetic clouds vs. high-turbulence conditions within corotating interaction regions.

An analytical estimate that includes both particle streaming along and diffusion perpendicular to the mean magnetic field (Equation 5 of Strauss et al. 2023) suggests that dispersion durations have a dependence proportional to magnetic connection distance to a higher power (e.g., 2). Such a dependence could match the observations better than the linear fits we used in Figure 4. However, given the limited number of events, in particular at larger connection distances, we have not considered here whether this or another dependence may provide a better fit to the observations. Fully understanding the variability of proton onset delays and energy dispersion durations at small magnetic connection distances requires further investigation.

We conclude that cross-field diffusion is a nonnegligible effect in the discussed proton energy range from $\approx 4.5-45$ MeV. This is not necessarily a contradiction to reports of "dropouts" in so-called impulsive ion events that are observed in the keV/n range. Since gyrocenters of these lower-energy particles move at only a few times the speed of the solar wind they are less likely to encounter scattering centers in the turbulent solar wind magnetic field than protons at much higher speeds, and their lower speeds do not allow them to move far away from their field line of origin before they reach 1 AU. A study that compares the longitudinal extents of MeV and keV/n ion events with energy dispersion using suitable instrumentation (i.e., measurements sufficiently free from cross-contamination of high- and low-energy ions) could resolve this question.

The need for large, expanded sources that accelerate protons to high energies is, in part, a conclusion from the observations of broad energetic particle events. We note, however, that a *rapid reduction* in magnetic field line length between the COB point and the observer from an expanding shock front is not supported by our result that shows that the duration of energy dispersion *increases* away from the source longitude. Neither is a scenario supported in which the expanding source simply expands in the lower solar corona (e.g., an EUV wave), i.e., without lifting the COB point into the heliosphere, as in this scenario the magnetic field line length to the observer will *stay the same*, independent of magnetic connection distance.

A feasible explanation of increasing energy dispersion duration with magnetic connection distance is a rather large role of cross-field diffusion between the accelerating source and the observer at 1 AU.

Appendix

A common occurrence among the events is the presence of a type III radio burst. We use the onset time of the detection of the type III radio burst in the frequency range of Wind/WAVES (20 kHz – 20 MHz) as a common reference start time of the event, as all other phenomena are either not present in all events (e.g., type II radio bursts) or not visible with common

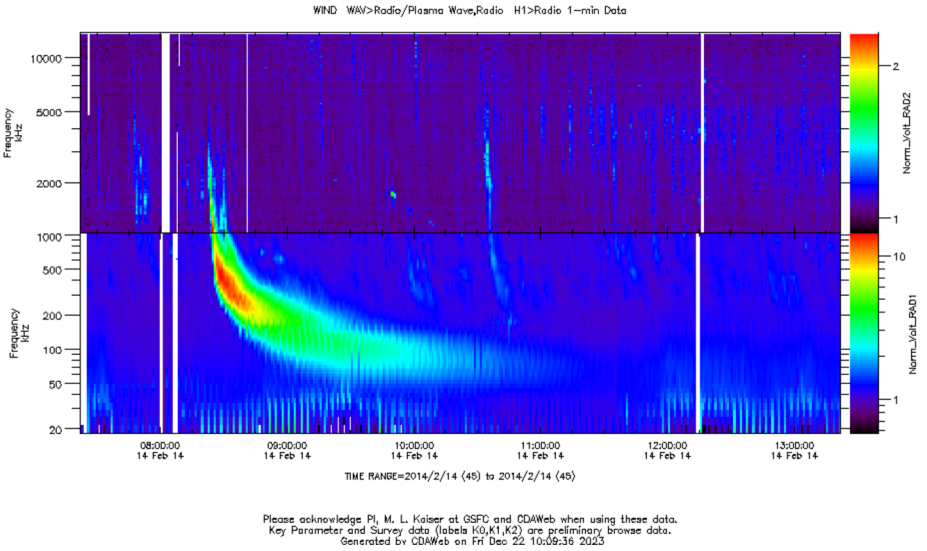

Figure A1 Radio observations on 14 Feb. 2014, by Wind/WAVES. The type III onset time (08:22 UT) has been entered in Table 1. This event corresponds to event No. 37 in Table 1.

instrumentation (e.g., X rays from the backside of the Sun as viewed from the Sun–Earth line).

Figure A1 shows the example of a type III radio burst that is associated with one of the 52 events of Table 1. The onset time of the type III radio burst can be determined to be within minutes accuracy, although some events have more than one bright type III, therefore the association itself can be ambiguous. All 52 individual SEP events listed in Table 1 did have significant type III radio bursts associated with them.

We also looked into the uncertainty of onset times of type IIIs observed at STEREO A and B as compared to Wind. A large and representative sample that includes events from all 12 source location sectors of Figure 5 shows that the uncertainty is under 2 minutes for most events, with the largest discrepancy at 7 minutes.

We noticed that for a small number of well-connected events, the orientation of the instrument with respect to the nominal magnetic field direction could affect the onset time and onset duration derivations. An example is that of event No. 41 in Figure A2. In the figure, a span of 24 hours is shown that includes onsets of two events, Nos. 41 and 42 of Table 1. The onset fit method for event No. 41 on the left suggests a rather brief dispersion feature. However, the intensity-time-profile fit is strongly influenced by the intensity enhancement observed at 02:42UT, or 3 hrs 20 min after the type III onset. This surge in proton intensity is observed in coincidence with the magnetic field direction rotation from 270° to within the EPHIN FOV, which is centered about 45°. The magnetic field is observed at the Advanced Composition Explorer (ACE) spacecraft, also in orbit around L1, as SOHO does not carry a magnetometer. This is a well-connected event; therefore, the expectation is that particle focusing would lead the first arriving protons to be nearly field aligned. Both events in this figure are observed when the instrument FOV is oriented perpendicular to the Parker spiral direction. Therefore, during the early phase of event No. 41, only a small fraction of arriving protons have sufficient pitch angle to be detected, leading to population 1. After the rotation, the bulk of arriving protons is observed (population 2). The spectrograms

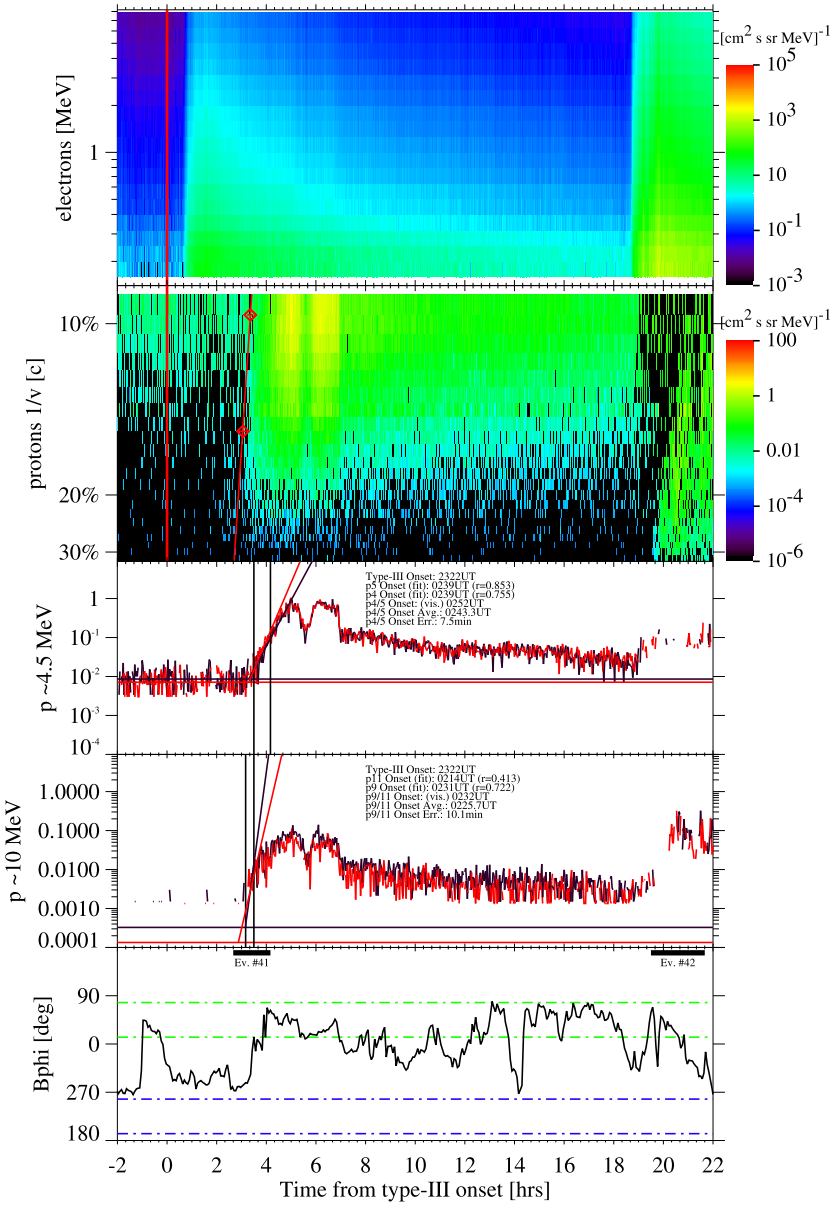

Figure A2 The top four panels have the same organization as Figure 1, but for events No. 41 and 42 in Table 1, for 24 hours starting on 28 March 2014, 21:22UT. The bottom panel shows the magnetic field azimuth (in GSE coordinates) measured by ACE. Ranges between like-color horizontal lines indicate the SOHO/COSTEP-EPHIN field of view range for field-aligned particles streaming anti-sunward. The approximate onset phases of SEP events No. 41 and 42 are highlighted by wide bars.

that identify the maximum energies to be around 40 MeV suggest that both populations are from the same source. Hence, the actual duration of energy dispersion is underestimated by the fitting method. We assume this effect diminishes with increasing magnetic connection

distance as the cross-field diffusion process preferentially affects protons with high pitch angles. The onset dispersion period of event No. 42 is also affected by a magnetic field fluctuation, occurring at 20:02 UT (or 20 hrs 40 min after the type III onset of event No. 41) but in the opposite way. Here, the pre-fluctuation flux of high-energy protons is directed into the instrument, while in the later phase the arriving low-energy protons are deflected away, causing a problem for accurately determination of the low-energy proton onset. Both events resulted in short 4.5 – 10 MeV dispersion-time outliers of the bottom panels of Figures 4 and 6.

Acknowledgements The authors thank the anonymous reviewers for their diligence, helpful comments, and suggestions. AP thanks Esayas Shume for discussions and helpful suggestions. AP dedicates the study to the memory of Dan Hirsch for many years of most dependable NASA IT support. SOHO is a project of international collaboration between ESA and NASA.

Author contributions AP wrote the main manuscript and analyzed SOHO data. IGR derived SEP source locations. RDTS supported the interpretation with modeling and theory. All three authors contributed to and reviewed the manuscript.

Funding IGR acknowledges support from NASA's Living With a Star Program grant NNH19ZDA001N-LWS and support from the STEREO mission. IGR and AP acknowledge support from the NASA Heliophysics Space Weather Research Program's CLEAR SWx Center of Excellence (PI Lulu Zhao) award 80NSSC23M0191. AP acknowledges support from the RadWorks project at NASA Johnson Space Center.

Data Availability SOHO/COSTEP-EPHIN level-1 data that are the basis for our energy dispersion duration analysis are available at http://ulysses.physik.uni-kiel.de/costep/level1/ All other data used are available from https://cdaweb.gsfc.nasa.gov/

Declarations

Competing interests The authors declare no competing interests.

References

Dresing, N., Rodríguez-García, L., Jebaraj, I.C., Warmuth, A., Wallace, S., Balmaceda, L., Podladchikova, T., Strauss, R.D.-T., Kouloumvakos, A., Palmroos, C., Krupar, V., Gieseler, J.: 2023, *Astron. Astrophys.* **674**, A105. DOI.

Gomez-Herrero, R., Dresing, N., Klassen, A., Heber, B., Lario, D., Agueda, N., Malandraki, O.E., Blanco, J.J., Rodriguez-Pacheco, J., Banjac, S.: 2015, *Astrophys. J.* **799**(1), 55.

Kallenrode, M.-B.: 1993, *J. Geophys. Res.* **98**, 5573.

Klein, K.-L., Posner, A.: 2005, *Astron. Astrophys.* **438**, 1029. DOI.

Kollhoff, A., Kouloumvakos, A., Lario, D., Dresing, N., Gómez-Herrero, R., Rodríguez-García, L., Malandraki, O.E., Richardson, I.G., Posner, A., Klein, K.-L., Pacheco, D., Klassen, A., Heber, B., Cohen, C.M.S., Laitinen, T., Cernuda, I., Dalla, S., Espinosa Lara, F., Vainio, R., Koeberle, M., Kuehl, R., Xu, Z.G., Berger, L., Eldrum, S., Bruedern, M., Laurenza, M., Kilpua, E.J., Aran, A., Rouillard, A.P., Bucík, R., Wijsen, N., Pomoell, J., Wimmer-Schweingruber, R.F., Martin, C., Böttcher, S.I., von Forstner,

J.L.F., Terasa, J.-C., Boden, S., Kulkarni, S., Ravanbakhsh, A., Yedla, M., Janitzek, N., Rodríguez-Pacheco, J., Prieto Mateo, M., Sánchez Prieto, S., Parra Espada, P., Rodríguez Polo, O., Martínez Hellín, A., Carcaboso, F., Mason, G.M., Ho, G.C., Allen, R.C., Andrews, G.B., Schlemm, C.E., Seifert, H., Tyagi, K., Lees, W.J., Hayes, J., Bale, S.D., Krupar, V., Horbury, T.S., Angelini, V., Evans, V., O'Brien, H., Maksimovic, M., Khotyaintsev, Y.V., Vecchio, A., Steinvall, K., Asvestari, E.: 2021, *Astron. Astrophys.* **656**, A20. DOI.

Kühl, P., Heber, B., Gomez-Herrero, R., Malandraki, O., Posner, A., Sierks, H.: 2020, *J. Space Weather Space Clim.* **10**, 53. DOI.

Laitinen, T, Dalla, S.: 2019, *Astrophys. J.* **887**, 222L. DOI.

Lario, D., Kwon, R.-Y., Richardson, I.G., Raouafi, N.E., Thompson, B.J., von Rosenvinge, T.T., Mays, M.L., Mäkelä, P.A., Xie, H., Bain, H.M., Zhang, M., Zhao, L., Cane, H.V., Papiouannou, A., Thakur, N., Riley, P.: 2017, *Astrophys. J.* **838**, 51. DOI.

Lin, R.P., Evans, L.G., Fainberg, J.: 1973, *Astrophys. Lett.* **14**, 191.

Mazur, J., Mason, G.M., Dwyer, J.R., Giacalone, J., Jokipii, J.R., Stone, E.C.: 2000, *Astrophys. J.* **32**, L79. DOI.

Müller-Mellin, R., Kunow, H., Fleißner, V., Pehlke, E., Rode, E., et al.: 1995, COSTEP–comprehensive suprathermal and energetic particle analyser. *Solar Phys.* **162**, 483. DOI.

Ogilvie, K.W., Chornay, D.J., Fritzenreiter, R.J., Hunsaker, F., Keller, J., Lobell, J., Miller, G., Scudder, J.D., Sittler, E.C., Torbert, R.B., Bodet, D., Needell, G., Lazarus, A.J., Steinberg, J.T., Tappin, J.H., Mavretic, A., Gergin, E.: 1995, *Space Sci. Rev.* **71**, 55. DOI.

Paassilta, M., Raukunen, O., Vainio, R., Valtonen, E., Papaioannou, A., Siipola, R., Riihonen, E., Dierckxsens, M., Crosby, N., Malandraki, O., Heber, B., Klein, K.-L.: 2017, *J. Space Weather Space Clim.* **7**, A14. DOI.

Paassilta, M., Papaioannou, A., Dresing, N., Vainio, R., Valtonen, E., Heber, B.: 2018, *Solar Phys.* **293**, 70. DOI.

Park, J., Innes, D.E., Bucik, R., Moon, Y.-J.: 2013, *Astrophys. J.* **779**(2), 184. DOI.

Pomoell, J., Poedts, S.: 2018, *J. Space Weather Space Clim.* **8**, A35. DOI.

Posner, A.: 2007, Space Weather **5**. DOI.

Posner, A., Arge, C.N., Staub, J., StCyr, O.C., Folta, D., Solanki, S.K., Strauss, R.D.-T., Effenberger, F., Gandorfer, A., Heber, B., Henney, C.J., Hirzberger, J., Jones, S.I., Kuehl, P., Malandraki, O., Sterken, V.J.: 2021, *Space Weather* 19. DOI.

Prise, A.J., Harra, L.K., Matthews, S.A., Long, D.M., Aylward, A.D.: 2014, *Solar Phys.* **289**(5), 1731. DOI.

Ragot, B.R.: 2006, *Astrophys. J.* **633**, 1493. DOI.

Reames, D.V., Barbier, L.M., Ng, C.K.: 1996, *Astrophys. J.* **466**, 473. DOI.

Richardson, I.G.: 2024, *Harvard Dataverse* **V1**,UNF:6:wDWbJQnOrrFoBOAs1wiZDw== [fileUNF]. DOI.

Richardson, I.G., von Rosenvinge, T.T., Cane, H.V., Christian, E.R., Cohen, C.M.S., Labrador, A.W., Leske, R.A., Mewaldt, R.A., Wiedenbeck, M.E., Stone, E.C.: 2014, *Solar Phys.* **289**, 3059. DOI.

Rouillard, A.P., Sheeley, N.R. Jr., Tylka, A., Vourlidas, A., Ng, C.K., Rakowski, C., Cohen, C.M.S., Mewaldt, R.A., Mason, G.M., Reames, D., Savani, N.P., StCyr, O.C., Szabo, A.: 2012, *Astrophys. J.* **752**, 44. DOI.

Strauss, R.D., Dresing, N., Richardson, I.G., van den Berg, J.P., Steyn, P.J.: 2023, *Astrophys. J.* **951**, 2. DOI.

Strauss, R.D., Fichtner, H.: 2015, *Astrophys. J.* **881**(1), 29. DOI.

von Rosenvinge, T.T., Reames, D.V., Baker, R., Hawk, J., Nolan, J.T., Ryan, L., Shuman, S., Wortman, K.A., Mewaldt, R.A., Cummings, A.C., Cook, W.R., Labrador, A.W., Leske, R.A., Wiedenbeck, M.E.: 2008, *Space Sci. Rev.* **136**, 391. DOI.

Wijsen, N., Aran, A., Scolini, C., Lario, D., Afanasiev, A., Vainio, R., Sanahuja, B., Pomoell, J., Poedts, S.: 2022, *Astron. Astrophys.* **659**, A187. DOI.

Zhao, L., Zhang, M.: 2018, *Astrophys. J. Lett.* **859**(2), L29. DOI.